X-621-68-369
PREPRINT

STRATOSPHERIC-MESOSPHERIC COUPLING DURING STRATOSPHERIC WARMINGS

HANS VOLLAND
GUENTER WARNECKE

SEPTEMBER 1968

GSFC
GODDARD SPACE FLIGHT CENTER
GREENBELT, MARYLAND

X-621-68-369
Preprint

STRATOSPHERIC-MESOSPHERIC COUPLING DURING STRATOSPHERIC WARMINGS

Hans Volland*

Guenter Warnecke†

Laboratory for Atmospheric and Biological Sciences

September 1968

GODDARD SPACE FLIGHT CENTER
Greenbelt, Maryland

---

*NAS-NRC Research Associate on leave from the Astronomical Institutes of the University of Bonn, Germany

† NAS-NRC Research Associate on leave from the Institute for Meteorology and Geophysics, Free University of Berlin, Germany

STRATOSPHERIC-MESOSPHERIC COUPLING DURING STRATOSPHERIC WARMINGS

Hans Volland* and Guenter Warnecke†

Laboratory for Atmospheric and Biological Sciences
Goddard Space Flight Center, Greenbelt, Md.

ABSTRACT

The thermal disturbance observed during the sudden stratospheric warming in January 1963 showed a wave-like behavior. The wave characteristics of this event were consistent with the propagation and attenuation of downward propagating turbulent heat conduction waves.

Full wave calculations indicate that the stratosphere behaves like a selective filter with respect to atmospheric waves. Waves can propagate northward only under the condition of a resultant southerly wind of about 5 m sec^{-1}. Upward propagating waves in the mesosphere are attenuated in such a manner that their relative amplitude generally does not increase with altitude. These considerations, in conjunction with the physical interpretation of observations of sudden stratospheric warmings and simultaneous short-period winter anomalies in the ionospheric D-region, lead to the suggestion of a common source, in form of a sudden initial heat impulse, of both phenomena. An upper limit for the generation of the initial heat impulse was placed at 50 km on the basis of observed wave characteristics and of static stability requirements in the polar winter mesosphere. Thus, the common source seems to be located at or a little below the stratopause.

---

*NAS-NRC Research Associate on leave from the Astronomical Institutes of the University of Bonn, Germany

† NAS-NRC Research Associate on leave from the Institute for Meteorology and Geophysics, Free University of Berlin, Germany

CONTENTS

		Page
ABSTRACT		iii
1.	INTRODUCTION	1
2.	TEMPORAL BEHAVIOR OF THE 1963 STRATOSPHERIC WARMING	2
3.	WAVE PARAMETERS DERIVED FROM TEMPERATURE OBSERVATIONS	4
4.	ORIGIN OF THE HEAT IMPULSE	7
5.	MECHANISM OF WAVE PROPAGATION WITHIN THE STRATOSPHERE	12
6.	THE ATMOSPHERE AS A SELECTIVE FILTER WITH RESPECT TO ATMOSPHERIC WAVES	18
7.	THE UPWARD TRANSPORT OF WAVE ENERGY	20
8.	CONCLUSIONS	22
9.	REFERENCES	33
APPENDIX A:	EIGENVALUES OF PLANE TURBULENT ATMOSPHERIC WAVES	25
APPENDIX B:	FULL WAVE THEORY AND RAY APPROXIMATION	29

STRATOSPHERIC-MESOSPHERIC COUPLING DURING STRATOSPHERIC WARMING

1. INTRODUCTION

From investigations by BOSSOLASCO and ELENA (1963) and others (SHAPLEY and BEYNON, 1965; LAUTER, 1967; BELROSE, 1967) it is now evident that sudden stratospheric warmings during winter, discovered by SCHERHAG (1952) show significant correlation with the increase of nondeviative absorption of medium and high frequency radio waves in the ionospheric D-region, known as winter anomaly of absorption, and with the simultaneous decrease of the virtual reflection height of LF- and VLF-waves. These ionospheric effects are believed to be closely related to changes in the neutral air properties, like temperature and pressure, and (or) variations of photochemical processes due to changes in large-scale neutral wind circulation during breakdown of the stratospheric polar vortex in the winter hemisphere (SECHRIST, 1967).

There remains the question of the origin of this disturbance and of the transport mechanism within the atmosphere. REGENER (1952) suggested already that the trigger mechanism for the stratospheric warming phenomenon may be located within the stratosphere, i.e., well below the ionospheric D-region, and FORTAK (1958) proposed a vertical turbulent heat transport as the propagation mechanism of the disturbance. These two suggestions will be considered in some detail in this paper. The wave structure of the sudden stratospheric warming phenomenon will be discussed quantitatively in terms of the event of January 1963. It will be shown that the disturbance originates from the region of higher temperature near the low latitude stratopause or even from the summer hemisphere, the

easterly circulation of which seems to expand abruptly toward the winter pole as a result of instabilities of the general wind system. Full wave calculations of turbulent atmospheric waves reveal that the characteristics of heat conduction waves are consistent with the observed wave structure during a sudden stratospheric warming.

2. TEMPORAL BEHAVIOR OF THE 1963 STRATOSPHERIC WARMING

One of the strongest stratospheric warmings ever observed occurred in January 1963. The synoptic features of this event have been described by FINGER and TEWELES (1964). The associated energy processes have been analyzed by JULIAN and LABITZKE (1965), PERRY (1967), and HIROTA (1967). This 1963 event was typical for strong stratospheric warmings. Temperature cross-sections and time-sections appeared to be very similar to the warmings in February 1952 (SCHERHAG, 1952) and January 1968 (FINGER and McINTURFF, 1968).

Figures 1a and 1b show temperature cross-sections along 90°W and 90°E during the maximum of stratospheric warming effect, on 26 January 1963, and six days earlier, on 20 January 1963, respectively. The data were taken and analyzed from a series of daily stratospheric maps published by the Institute for Meteorology and Geophysics, Free University of Berlin (METEOROLOGISCHE ABHANDLUNGEN, 1963-1966) and from WARNECKE (1968). Although the isothermal planes of the disturbance are tilted not only toward the north but also toward the west and propagate toward the northwest, changing the direction of propagation with time, the tilt and the direction of propagation are predominantly northward. Therefore, we consider a meridional cross section only. Figure 2

shows the stratospheric temperature variation with time for a number of isobaric levels above the location 70°N, 90°W, near the center of maximum warming. From this figure, the time of occurrence of the maximum temperature as a function of isobaric level was determined and plotted, Figure 3, versus height (filled-in circles). The horizontal solid bars indicate the estimated range of uncertainty of the observations. The open circles and the horizontal dashed bars have been derived from the observations of the Berlin Warming in February 1952 (FORTAK, 1958).

In Figure 4 the decrease of the relative amplitude $\Delta T/\overline{T}$, normalized by the 10mb value, has been plotted versus height. Here $\overline{T}$ (in degrees Kelvin) is a reference temperature, defined as the average of the observed equilibrium temperatures before and after the warming phenomenon. ΔT is the maximum deviation from the reference temperature $\overline{T}$. Since the equilibrium temperatures before and after the warming phenomenon are not very well defined in the observations, the range of estimated uncertainty of the derived parameters is indicated by solid bars in Figure 4. The open circles and the dashed bars again represent data derived from the 1952 warming. Since this event has been observed over Berlin, Germany, i.e., at one random location, only, while the data of the 1963 warming were taken at the well defined location of maximum effect, some precaution is advisable in comparing the absolute values of the parameters derived for the two events. But nevertheless, very similar features can be seen in Figures 3 and 4. The larger time delay in the occurrence of the temperature maximum as well as a stronger decrease of the temperature amplitude with decreasing height was observed in case of the 1952 warming.

3. WAVE PARAMETERS DERIVED FROM TEMPERATURE OBSERVATIONS

The history of the 1963 stratospheric warming at different altitudes, as demonstrated in Figure 1, suggests that this phenomenon be treated theoretically as wave-like propagation of an impulse type disturbance. The main task pursued in this study was to determine the wave mode involved from the observations. As a first approach, the discussion was confined to the highly idealistic model of plane free internal harmonic waves extended infinitely in the horizontal and vertical directions. Such waves can be described by the expression

$$e_1 = e_0 \, e^{j\omega t - jk_x x - jk_z z + \frac{z}{2H}} \tag{1}$$

where t is time, ω is angular frequency.

$$k_x = \frac{\omega}{V_x} \tag{2}$$

is the horizontal wave number which is assumed to be real and constant, V_x is the horizontal phase velocity. A real and constant value of k_x is suggested from the temporal and spatial behavior of the observed disturbance, which propagates with fairly constant horizontal velocity and with only slight changes of its shape (see Figures 1a and 1b).

$$k_z(z) = k_{zr} - j k_{zi} \tag{3}$$

is a complex vertical wave number, with $j = \sqrt{-1}$.

$$k_{zr}(z) = \frac{\omega}{V_z(z)} \tag{4}$$

is the real part of k_z. The altitude dependence of k_{z_r} involves diffraction of the waves and therefore a bending of the wave planes. V_z is the vertical phase velocity. $k_{z_i}(z)$ is the negative imaginary part of k_z, responsible for the dissipation of wave energy in the direction of propagation. Therefore k_{z_i} is positive for waves propagating upwards (transporting energy upwards) and is negative for waves propagating downward. The wave amplitudes of our wave modes are normalized in such a manner that their squared magnitude is a measure of wave energy (see Appendix B). Therefore a term 1/2H has been added in the exponent in Equation (1), where H is the scale height. This takes into account the adiabatic increase with height of the amplitudes of physical parameters like relative temperature disturbance $\Delta T/\overline{T}$ or relative pressure disturbance $\Delta p/\overline{p}$ within an isothermal atmosphere. Thus

$$\frac{1}{2H} - k_{z_i} \begin{cases} < \\ > \end{cases} \frac{1}{2H} \text{ for } \begin{cases} \text{upgoing waves} \\ \text{downgoing waves} \end{cases} \tag{5}$$

may be larger or smaller than zero for upgoing waves indicating an increase or decrease of the relative amplitudes with height. Downward propagating waves always show a decrease of amplitude in the direction of wave propagation.

According to Figure 1, the actual wave structure is considerably more complicated than assumed in the plane wave model. In fact, the horizontal and vertical velocities of the disturbance determined from Figure 1 are group velocities rather than phase velocities. Furthermore, the wave is attenuated not only in the vertical but also in the horizontal direction, suggesting spherical waves rather than plane waves. Therefore, only qualitative agreement between the wave characteristics derived from Figure 1 and the theoretical model, outlined in section 4, can be expected.

From Figures 1 to 4 the following wave characteristics were determined:

(a) components of the mean group velocities, supposed to be nearly equal to the phase velocities

$$V_x \sim 4.5 \times 10^{-3} \text{ km sec}^{-1}$$
$$V_z \sim 2.5 \times 10^{-5} \text{ km sec}^{-1}; \tag{6}$$

(b) mean angle of incidence:

$$\theta = \arctan \frac{V_z}{V_x} \sim 0.^{\circ}32; \tag{7}$$

(c) the predominant angular frequency of the impulse:

$$\omega \sim \frac{2\pi}{\Delta\tau} \sim 7 \times 10^{-6} \text{ sec}^{-1} \tag{8}$$

where $\Delta\tau \sim 10$ days is the width of the impulse.

From Equations (2), (4), (6), and (8) it follows that

$$k_x \sim 1.5 \times 10^{-3} \text{ km}^{-1}$$
$$k_{zr} \sim 0.28 \text{ km}^{-1} \tag{9}$$

For comparison, the westward tilt given by HIROTA's (1967b) Figures 3c and 3d along the 50°N latitude circle is

$$\theta \sim 0.^{\circ}13$$

and the horizontal west component of the velocity of the disturbance is

$$V_x \sim 2.1 \times 10^{-3} \text{ km/sec}.$$

These data are smaller than the values of the north components by a factor of more than 2 and become even smaller near the center of the disturbance. This justifies neglecting the western component of the disturbance in our calculations.

From Figure 4 and Equation (5) we find the mean value of the attenuation rate as

$$k_{zi} \sim -0.05 \text{ km}^{-1}. \tag{10}$$

The dashed line in Figure 4 is related to the amplification of waves according to the term 1/2 H. Since the observed attenuation rate is negative, and therefore

$$\frac{1}{2H} - k_{zi} > \frac{1}{2H}, \tag{11}$$

it can immediately be concluded, from Equations (5) and (11), that the wave propagates downward, transporting energy in the downward direction.

4. ORIGIN OF THE HEAT IMPULSE

A complete theory of the sudden stratospheric warming phenomenon has to explain not only the wave structure, discussed in the previous sections, but also the origin, shape, and direction of propagation of the heat impulse. Due to the lack of comparative observational data, the quantitative investigation in this paper was mainly restricted to propagation characteristics of the predominant wave.

With regard to the spatial origin of the heat impulse, only a more or less qualitative estimate on the initial altitude was possible on the basis of the discussed wave theory and sparse observations.

SHAPLEY and BEYNON (1965) found no time lag between stratospheric temperature changes at 31 km and simultaneous D-region absorption events. They suggested a common source for both phenomena at an intermediate altitude. LAUTER (1967) however, found that the D-region abnormal absorption preceeds the maximum of the stratospheric warming event by one or two days. From analysis of significantly correlated stratospheric and ionospheric data obtained over Canada, MANSON (1968) concluded that the origin of the disturbance is above 25 km. The data presented in Figure 1 of this paper and the interpretation of the warming as a wave-like phenomenon suggest an origin at or above the top level of the presented observational data, i.e., at or above the 10 mb level or 31 km altitude. In the following, an estimate of the height of origin of the initial heat impulse on physical grounds will be attempted.

Considering a downward propagating attenuated wave and a lower limit of the decrease of relative amplitude of temperature with decreasing altitude, it is

$$\frac{\Delta T}{\bar{T}}\Big|_{z_0} > \frac{\Delta T}{\bar{T}}\Big|_{z} e^{-\int_{z_0}^{z} \frac{d\xi}{2H}} \qquad (12)$$

according to Equation (5). Since during stratospheric warmings temperature increases of 50°K have been observed near 30 km (WARNECKE, 1962), the vertical distribution of the lower limit of relative temperature amplitude, represented in curve A of Figure 5, was based on this value for 30 km altitude. This value will

certainly be on the low side because of the incompleteness of observational data. It can be deduced from this figure that a minimal initial temperature impulse of 100°K at 40 km, 185°K at 50 km, or 370°K at 60 km were necessary to explain the observed amplitude of at least 50°K at 30 km. These altitudes are, however, beyond the top altitude of present routine networks of sufficiently dense observations in space and time. Thus no complete survey on actual absolute temperature amplitudes above 35 kilometers, associated with sudden stratospheric warmings, is available for an exact determination of the vertical and horizontal localization of the initial heat impulse. A temperature increase of nearly 40°K was observed by SECHRIST et al. (1968) between 40 km and 50 km and between 75 and 85 km at Wallops Island, Virginia, during rapid changes in D-region absorption. JONES et al. (1959) reported a temperature increase of 58°K within four days observed at 40 km over Churchill, Manitoba. During the recent 1967/68 stratospheric warming (JOHNSON, 1968) British rocket measurements over West Geirinish, Hebrides revealed a maximum temperature change of nearly 90°K around 43 km altitude from the warming peak toward the post-warming temperature level (LABITZKE and SCHWENTEK, 1968). Unfortunately, no measurements were taken during the pre-warming period.

These observed values, even the latter one, may, however, still be far from the total maximum temperature amplitude during sudden stratospheric warmings, because in all three cases neither the entire warming period nor the region of maximum warming was covered by the rather sporadic observations. Thus, these data should be considered more as minimal values.

An upper physical limit for a temperature increase in the lower mesosphere or at the stratopause level is given by hydrostatic stability conditions, i.e., by

the dry adiabatic lapse rate which cannot be exceeded. Assuming an isothermal mesosphere, which is fairly realistic during winter over higher mid-latitudes between 50 km and 70 km (SMITH, et al., 1967), a temperature increase by 200°K at 50 km altitude is permissible before vertical instability throughout the major parts of the mesosphere occurs. This is illustrated by curve B in Figure 5 which represents the permissible temperature increase as a function of height in an atmosphere of zero vertical lapse rate between 50 and 70 km. Below 50 km allowance was made in curve B for a subsidence of the stratopause during the warming process, i.e., the permissible temperature rise increases more strongly below the stratopause because of the lower temperatures in the stratosphere.

As curve B represents maximum values, curve A minimum values, one basic conclusion can be drawn from Figure 5: the altitude of origin of the initial heat impulse cannot be higher than 50 kilometers, the altitude of the cross-over point of both curves, and the height of the origin as well as the initial amplitude of the heat impulse can very likely be expected within the hatched region of Figure 5.

While the vertical localization of the origin of the heat impulse could at least be estimated by physical reasoning, a discussion of its geographic origin and of its physical nature would become rather speculative.

From a meridional temperature cross-section it can be learned that the layer of high temperature, centered at the stratopause and caused by absorption of solar ultraviolet radiation by atmospheric ozone, fades out toward the winter pole and does not exist during polar night poleward of 65° latitude (COLE and CANTOR, 1963). During a sudden stratospheric warming the polar vortex, which prevents a direct (advective) latitudinal stratospheric heat exchange within the

stratopause layer, breaks down. This break-down presently is assumed to be caused by baroclinic instability processes within an irregularly shaped vortex (MATSUNO and HIROTA, 1966). But barotropic processes were also suggested (JULIAN and LABITZKE, 1965) to accomplish the accumulation of energy available for sudden release into sensible heat during the warming event. Recent numerical experiments with a rather sophisticated multi-layer atmospheric model by MIYAKODA et al. (1968) were successful in simulating the split of the polar vortex, which usually is associated with sudden warmings, but failed to produce the sudden stratospheric warming itself out of the baroclinic model. The MIYAKODA experiment also showed that barotropic processes were insignificant for the polar vortex break-down and the warming phenomenon as well.

Whether the failure of the simulation experiment was due to residual incompleteness of the atmospheric model used or the sudden stratospheric warming phenomenon is predominantly caused by a yet undetected process or group of processes could not be solved. The MIYAKODA Experiment showed, however, that barotropic processes were insignificant for the polar vortex break-down and the warming phenomenon as well. Thus the process of generation of the heat impulse is still unknown. HIROTA, 1967b pointed out that the downward propagation of the disturbance during the 1963 warming was preceded by an upward motion of a warming process from the 100 mb or 50 mb level into the 10 mb region. He, therefore, distinguishes between an intensification stage, during which the disturbance propagates upward from the lower into the upper stratosphere, and a migration stage, during which the disturbance propagates toward the pole and downward, in connection with the break-down of the polar vortex. The first stage, between 11 and 15 January 1963 in his case, might act as a

trigger mechanism for the second stage, but is certainly not a thermal source of the heat energy observed during the migration stage because its heat energy content is only a fraction of the heat energy exhibited during the second stage [see for example our Figure 2 or HIROTA's (1967b) Figure 5].

Because of these uncertainties in the present understanding of the generation mechanism of the initial heat impulse during sudden stratospheric warmings, this investigation was concentrated on the second stage, in HIROTA's sense, i.e., the migration stage, which so vehemently performs transport of heat energy toward the winter pole and represents one of the most drastic mechanisms of heat exchange between the sunlit and the polar night sections of the earth's atmosphere. This energy flow has an impulse shape due to the finite abundance of thermal energy within the stratopause region. We consider this energy as the generator of a spectrum of atmospheric wave modes which propagate in all possible directions. The response of the stratosphere and the mesosphere to these waves, depending on frequency and angle of incidence, will be discussed in the following sections.

5. MECHANISM OF WAVE PROPAGATION WITHIN THE STRATOSPHERE

The atmosphere below 100 km is in a highly turbulent state. This can be described in a first order approximation by a frequency dependent turbulent diffusion coefficient. For periods of more than a day, the turbulent diffusion coefficient within the stratosphere and mesosphere is about 10^3 times larger than the molecular diffusion coefficient of air (KELLOGG, 1964; NEWELL, 1963). Eddy viscosity and eddy heat conduction are linearly related to the eddy diffusion coefficient. If we assume the factors of proportionality between these

three coefficients to be of the same order of magnitude as the corresponding molecular coefficients, the coefficient of eddy heat conductivity within the stratosphere becomes

$$\kappa_{eddy} = A\sqrt{\overline{T}} \sim 3.5 \times 10^{6} \text{ erg cm}^{-1} \text{ sec}^{-1} \text{ deg}^{-1} \qquad (13)$$

with $A = 2 \times 10^{5}$ erg cm^{-1} sec^{-1} $deg^{-3/2}$ and an eddy coefficient of viscosity of

$$\eta_{eddy} = 8 \times 10^{-2}\sqrt{\overline{T}} = 0.14 \text{ g cm}^{-1} \text{ sec}^{-1} . \qquad (14)$$

The exact numerical value of κ_{eddy} is, however, not very critical for the following discussion, as will be shown later.

It was shown by VOLLAND (1968a) that in the treatment of the propagation of plane internal harmonic waves the coefficient of viscosity can be neglected as compared with the coefficient of heat conductivity at very low frequencies [see for example, the condition in Equation (A-1)]. This leads to the predominance of two wave types in the atmosphere: gravity waves and heat conduction waves. The dispersion formula of these two waves can be found in Appendix A, Equation (A-2). Both wave types are coupled with each other, in a realistic atmosphere. In order to find the wave pattern of these waves and their relative importance, a full wave calculation must be performed. Some basic information about full wave analysis is outlined in Appendix B.

For the full wave calculation, performed in the following, numerical values for the atmospheric parameters, like mean pressure $\overline{p}$, mean temperature $\overline{T}$, and velocity of sound C, were taken from CANTOR and COLE (1963). Considering

descending waves $b^j \neq 0$ at an altitude of $z_j = 31$ km (10 mb level), we ask for the descending waves b^i at $z_i = 16$ km (100 mb level) under the assumption that the ascending waves disappear at this altitude ($a^i = 0$). The ascending waves at the altitude z_j are then, following Equation (B-3),

$$a^j = R^j b^j . \tag{15}$$

We now specify the descending waves b^j either as a gravity wave ($b_G^j \neq 0$) or a heat conduction wave ($b_H^j \neq 0$). From Equations (B-1), (B-4), and (15) the physical parameters at the altitude z_i follow as

$$e^{i\nu} = \left(\frac{Q}{\sqrt{\bar{p}\, C}} \right)_i P^{ij}\, c^{j\nu} \tag{16}$$

where

$$c^{j1} = \begin{pmatrix} {}_G R_G^j \\ {}_H R_G^j \\ 1 \\ 0 \end{pmatrix} b_G^j \quad \text{for gravity waves} \tag{16a}$$

or

$$c^{j2} = \begin{pmatrix} {}_G R_H^j \\ {}_H R_H^j \\ 0 \\ 1 \end{pmatrix} b_H^j \quad \text{for heat conduction waves} \tag{16b}$$

Numerical results of Equation (16) are given in Figure 6. Here the following values of parameters k_x, ω, and κ_{eddy} from Equations (8), (9), and (13) have been used:

$$k_x = 1.5 \times 10^{-3}\ \mathrm{km}^{-1}$$

$$\omega = 7 \times 10^{-6}\ \mathrm{sec}^{-1}$$

$$\kappa_{eddy} = 2 \times 10^{5} \sqrt{\overline{T}}\ \mathrm{erg\ cm}^{-1}\ \mathrm{sec}^{-1}\ \mathrm{deg}^{-1}\ .$$

The dispersion equation, Equation (A-2), depends on the Coriolis parameter f. However, since the discussed stratospheric warming phenomena occurred only over the northern winter hemisphere, and the Coriolis parameter is not of great influence on the vertical wave number k_z within the considered range of ω_{eff} and k_x, the parameter f has been chosen constant and the value for 45°N has been adopted as representative, in this case.

Figure 6a gives the amplitude B of the relative temperature disturbance at the altitude z_i, normalized to the value at altitude z_j, which is

$$\frac{(\Delta T/\overline{T})_{z_i = 16\ \mathrm{km}}}{(\Delta T/\overline{T})_{z_j = 31\ \mathrm{km}}} = B\, e^{j\Phi}, \qquad (17)$$

as a function of effective angular frequency ω_{eff}. Figure 6b shows its phase Φ, where the right ordinate scale is the vertical travel time of the wave crest which is considered to be almost equal to the time delay

$$\Delta t = -\frac{\Phi}{\omega}\ . \qquad (18)$$

The lines marked by "GR" in this figure have been calculated from Equation (16a) and are related to an initial gravity wave; the lines marked by "HC" have been calculated from Equation (16b) and are related to an initial heat conduction wave.

Comparing the data in Figure 5 with the observed values presented in Figures 3 and 4, a best fit for an initial heat conduction wave was found for

$$\omega_{eff} = 4.6 \times 10^{-8} \text{ sec}^{-1}. \tag{19}$$

In Figures 3 and 4, the solid lines labelled as I represent theoretical values calculated from Equations (16) and (16b). While the theoretical curve in Figure 3 fits well the observed January 1963 values of time delay of the occurrence of temperature maximum with decreasing height, the theoretical (solid) curve I in Figure 4 indicates a larger decrease of relative temperature amplitude with decreasing altitude than observed during the 1963 warming. This suggests a larger attenuation rate of the temperature disturbance.

A better fitting pair of curves, the dashed lines labelled as II in Figures 3 and 4, are theoretical curves calculated with slightly changed wave parameters:

$$\begin{aligned} \omega &= 5 \times 10^{-6} \text{ sec}^{-1} \\ k_x &= 1 \times 10^{-3} \text{ km}^{-1} \\ \omega_{eff} &= 2.2 \times 10^{-8} \text{ sec}^{-1}. \end{aligned} \tag{20}$$

The assumed value for ω is equivalent to an impulse bandwidth of $\Delta\tau \sim 1/\omega$ = 15 days, which is somewhat larger than the observed value of $\Delta\tau \sim 10$ days. This discrepancy between observation and theory is not surprising in view of the rather primitive theoretical model. In this connection it might be emphasized that the theory presented, which is based on a strict perturbation method, neglects higher order terms of the perturbation parameters ΔT or Δp. Thus, the theory

cannot predict the heating of surrounding air due to dissipation of the penetrating wave. It may, therefore, be expected that the theoretical dissipation rate is larger than the real dissipation. These considerations seem to point into the right direction in order to explain and correct for the discrepancy mentioned above.

From Figure 5 we see a quasi-linear relationship between time lag Δt and attenuation rate of $(\Delta T/\overline{T})$ for heat conduction waves. This relationship can be qualitatively verified in Figures 3 and 4. The time lag and the attenuation rate of the January 1963 warming were smaller than the corresponding values of the February 1952 event, as suggested from Figure 5.

The numerical value of ω_{eff} in Equation (19) is equivalent to a mean southerly wind of

$$\overline{u}_x = \frac{\omega - \omega_{eff}}{k_x} \approx 4.5 \times 10^{-3} \text{ km sec}^{-1} .$$

Since $\omega >> \omega_{eff}$, the exact numerical value of ω_{eff} has not much influence on $\overline{u}_x$. Moreover, from Equation (A-2) it follows that ω_{eff} exists only in the product $\omega_h \omega_{eff}$. Therefore, a change in the numerical value of the austausch coefficient κ_{eff}, which is inverse by proportional to ω_h, influences merely the numerical value of ω_{eff} but does not significantly change the result of the foregoing discussion.

In Figure 6, the dashed lines have been calculated from the Wentzel- Kramer-Brillouin (WKB-) approximation [Equation (B-6)]. The close agreement of the dashed and the solid lines, calculated from full wave analysis in the frequency range $10^{-8} < \omega_{eff} < 10^{-7}$ sec^{-1}, in Figure 5 indicates that coupling and reflection

are of minor importance in this frequency range and that the nature of the wave type does not significantly change during downward propagation.

In Figures 1a and 1b the dash-dotted lines are planes of equal phase of the downward propagating heat conduction wave calculated from the WKB solution [Equation (B-3)] using the wave parameters of Equation (20). They agree with the observed location of the wave crust of the impulse type disturbance.

It can therefore be concluded from Figures 1, 3, 4, and 5 that the hypothesis of downward propagating heat conduction waves through an atmosphere exhibiting a resultant southerly wind in the order of 5 m sec^{-1} is consistent with the observed wave-like pattern of the three-dimensional temperature field during sudden stratospheric warmings in the northern hemisphere in winter.

6. THE ATMOSPHERE AS A SELECTIVE FILTER WITH RESPECT TO ATMOSPHERIC WAVES

In section 5 it has been shown that descending plane harmonic heat conduction waves of angular frequency $\omega = 7 \times 10^{-6}$ sec^{-1} propagating under a certain angle of incidence (horizontal wave number $k_x = 1.5 \times 10^{-3}$ km^{-1}) are consistent with the observed wave like pattern of the temperature field during sudden stratospheric warmings. There remains the question why these waves possess just these values of ω and k_x.

The impulse shape and the direction of energy flow depend on the impulse generator, its antenna characteristics and of the response of the surrounding atmosphere to the generated atmospheric wave modes. The determination of the impulse generator and its antenna characteristics is outside the scope of this

paper. We only can suggest from the observations that the generator creates a single impulse with a bandwidth of about 10 days and that the antenna beam is mainly directed toward the winter hemisphere. Moreover, we can expect that evanescent waves (having nearly zero real vertical wavenumber) are much less excited by the "antenna" than the propagation modes.

In order to determine the influence of the atmosphere on the wave propagation full wave calculations of the kind described in section 5 have been repeated for the same atmospheric model ($16 \leqq z \leqq 31$ km) and for downward propagating waves. The results are plotted versus horizontal wavenumber k_x in Figure 7. Here, the parameter is the effective angular frequency ω_{eff}. We notice from Figure 7 that the amplitude of the temperature disturbance decreases with increasing k_x and increasing ω_{eff}. The amplitude of the heat conduction wave has dropped to the value $\leqq 10^{-2}$ at $\omega_{eff} \geqq 10^{-8}$ sec^{-1} and $k_x \geqq 2 \times 10^{-2}$ km^{-1}. The stratosphere therefore prevents the downward propagation of heat conduction waves in these ranges of k_x and ω_{eff}.

With decreasing ω_{eff} and k_x the phase angles of the disturbance approach the value zero which indicates that in this range heat conduction waves behave like evanescent waves. The excitation of evanescent waves by a generator imbedded within the atmosphere is not very likely. Therefore in the ranges $\omega_{eff} < 10^{-8}$ sec^{-1}, $k_x < 10^{-4}$ km^{-1} we expect again only a small amount of energy from downward propagated heat conduction waves.

For gravity waves the same arguments are true in an even stronger sense. At small horizontal wave numbers ($k_x < 10^{-3}$ km^{-1}) gravity waves are of an evanescent type. At higher values of k_x ($> 10^{-3}$ km^{-1}) gravity waves are either

attenuated more strongly than heat conduction waves (at $\omega_{eff} < 10^{-7}$ sec^{-1}) or their amplitude has dropped by more than 10^{-2} (at $\omega_{eff} \gtrsim 10^{-7}$ sec^{-1}).

Therefore we conclude that downward wave propagation within the stratosphere is possible mainly by heat conduction waves with a predominant horizontal wave number of the order of $k_x \sim 10^{-3}$ km^{-1} and a predominant effective angular frequency of $\omega_{eff} \sim 10^{-8} - 10^{-7}$ sec^{-1} which is consistent with the observations. The limitation to a certain value of ω_{eff} equivalent to a mean horizontal southerly wind of the order of 5 m/sec suggests that it might be this last condition — namely the southerly wind of that strength — which triggers the energy transport. If the wind blows from the north, no turbulent heat conduction wave can propagate downward into the lower stratosphere.

The appropriate conditions for the triggering wind system may, perhaps, be established by the intensification stage, defined by HIROTA (1967b), of the warming phenomenon.

7. THE UPWARD TRANSPORT OF WAVE ENERGY

We finally ask about the upward transport of wave energy. For this reason we have calculated in Figure 8 the ratio between the relative temperature disturbances in $z_j = 70$ km and in $z_i = 45$ km height versus horizontal wavenumber k_x in the same manner as in Figure 7. The variable parameter is again the effective angular frequency ω_{eff}. Here the calculations are based on the assumption that at the lower height z_i a gravity wave (GR) or a heat conduction wave (HC) create a temperature disturbance of the amplitude one and that at the altitude z_j no descending wave exists.

From Figure 8 we notice that the amplification of the relative temperature disturbance generally does not exceed the factor 1.5. Only gravity waves at vertical incidence ($k_x < 10^{-4}$ km^{-1}) and low frequencies ($\omega_{eff} < 10^{-7}$ sec^{-1}) have higher values. Heat conduction waves with high horizontal wave numbers and high frequency ranges ($k_x > 10^{-2}$ km^{-1}; $\omega_{eff} > 10^{-8}$ sec^{-1}) as well as waves with small horizontal wavenumbers and low frequencies ($k_x < 10^{-3}$ km^{-1}; $\omega_{eff} < 10^{-8}$ sec^{-1}) can be excluded as participating in an effective upward energy transport and there remains a range around $\omega_{eff} \sim 10^{-7}$ sec; $k_x \sim 10^{-3} - 10^{-2}$ km^{-1} for the propagation modes. However, the predominance of gravity waves at vertical incidence ($k_x < 10^{-4}$ km^{-1}) in the upward energy transport can not be excluded.

LAUTER (1967) observed that the phenomenon of the winter anomaly is increasing with height and that it has perhaps a maximum in the 100 km height region. Figure 9 shows the relative temperature disturbance as function of the upper boundary z_j of our model normalized again by the temperature disturbance in 45 km height. The curves marked by "GR" are for gravity waves with the parameters $\omega_{eff} = 10^{-7}$ sec^{-1}; $k_x = 10^{-5}$ km^{-1}, those marked by "HC" are for heat conduction waves with the parameters $\omega_{eff} = 10^{-7}$ sec^{-1}; $k_x = 10^{-3}$ km^{-1}. In these calculations the factor A of the coefficient of heat conductivity has been taken as constant and of the value shown in Equation (13), below an altitude of 85 km. Above 85 km, the value A drops linearly to the value $A = 2 \times 10^2$ erg/cm sec deg of the molecular heat conductivity. The amplitudes of both waves show a maximum between 80 and 90 km which is due to the decrease of κ_{eddy} above this region. The time lag at 65 km height is 2.5 days for heat conduction waves and 4 days for gravity waves and remains nearly constant below 100 km altitude. We

compare this time with the travelling time of downward propagating heat conduction waves, considered in Figures 3 and 4, between 45 and 30 km, which is about 5 days.

From correlation studies between sudden stratospheric warmings and winter anomalies in the ionospheric D-layer it has been found that the maximum of the winter anomaly event preceeds the maximum of the stratospheric warming event by some days (LAUTER, 1967). During a winter anomaly SECHRIST et al. (1968) observed a temperature disturbance within the ionospheric D-region which had an impulse shape with maximum amplitude of the order of 50°C. Both observations are in general agreement with what we expect from the amplitudes and from the time of phase lag in Figures 7, 8 and 9, though it is, of course, presently impossible to draw more than very crude conclusions from a comparison between the sparse observational data and the theoretical calculations.

8. CONCLUSIONS

The wave-like appearance of the temperature disturbance during the sudden stratospheric warming phenomenon of January 1963 can be described by a downward propagating plane turbulent heat conduction wave of angular frequency $\omega = 7 \times 10^{-6}\,\mathrm{sec}^{-1}$ (equivalent to an impulse width of $\Delta\tau = 10$ days) and of horizontal wave length $\lambda_x = 4200$ km (equivalent to a horizontal wave number $k_x = 1.5 \times 10^{-3}\ \mathrm{km}^{-1}$). Computations of the horizontal and the vertical phase velocity as well as the dissipation rate of the wave amplitude using these wave parameters agree with values derived from observation. In these calculations, turbulence has been introduced by a turbulent austausch coefficient 10^3 times larger than the molecular coefficient of heat conductivity. However, a necessary condition for

agreement between theory and observation is the required existence of a mean southerly wind of the order of 5 m sec^{-1}, in order to meet the special wave characteristics. This mean wind field is suggested to be the triggering mechanism of the wave propagation observed during sudden stratospheric warmings; it might be established by processes involved in the intensification period recently revealed by HIROTA (1967b). In case of a mean northerly wind, downward propagation of waves would be prevented, according to the wave theory.

From energy and vertical stability considerations it can be concluded that the generator for this wave propagation, the production of the initial heat impulse, must be located below 50 kilometers, i.e., at or below the stratopause.

The calculation of upward wave propagation from 45 km to 110 km shows first a slight increase and then a decrease of the relative wave amplitude, with a maximum at 85 km. This maximum results from the transition from eddy heat transport to molecular heat conduction near the turbopause. The time of arrival at an altitude of 75 km is about half the propagation time of downward propagating waves between 45 km and 30 km the time difference being some days. Both findings are consistent with observations of the short period winter anomalies in the ionospheric D-region.

Thus, both the observed propagation of sudden stratospheric warmings and the observed associated effects of increased D-layer absorption can be understood as consequences of a sudden heat impulse released near the stratopause. The calculations were based on simple plane harmonic waves; sudden stratospheric warmings, however, actually have an impulse structure. Thus, an exact theoretical treatment of the impulse propagation will certainly modify the numerical

results. Knowledge of the generation mechanism and of the "antenna characteristics" of the generator within the stratopause layer will, however, be required in order to accomplish this treatment, which therefore, has to be postponed until appropriate observational data become available.

Appendix A

EIGENVALUES OF PLANE TURBULENT ATMOSPHERIC WAVES

It can be shown (VOLLAND, 1968a) that the coefficient of viscosity η is negligible as compared with the coefficient of heat conductivity κ in the treatment of the propagation of free internal plane harmonic waves through an isothermal atmosphere as long as the conditions

$$\omega_h > \omega_a > \frac{k_x^2 C^2}{\omega_{eff}} \qquad \text{(A-1)}$$

hold. It is

$\omega_{eff} = \omega - k_x \bar{u}_x$ effective angular frequency

ω angular frequency

$\bar{u}_x$ mean horizontal wind velocity in the direction of wave propagation (x-direction of a Cartesian coordinate system)

k_x horizontal wave number

$\omega_h = \frac{\gamma g}{2 V}$

$\omega_a = \frac{\gamma g}{2 C}$

$\gamma = \frac{c_p}{c_v}$ ratio between the specific heats at constant pressure and at constant volume

g gravitational constant

C velocity of sound

$V = \frac{\kappa\, g}{c_p\, \bar{p}}$ heat conduction velocity

κ coefficient of heat conductivity

$\bar{p}$ mean pressure

$\bar{T}$ mean temperature.

Under these circumstances the viscosity waves are decoupled from the gravity and from the heat conduction waves. Viscosity waves are heavily attenuated and do not contribute very much to the energy transport.

Taking into account the unequalities in Equation (A-1) we find the vertical wave number k_z of the predominant gravity waves and heat conduction waves from Equation (44) in VOLLAND (1968a)

$$Ck_{z\nu} = -j\sqrt{\omega_a^2 + j\omega_h\omega_{eff}\left(1 \mp \sqrt{1 + \frac{2j k_x^2 C^2 \omega_g^2}{\omega_h\omega_{eff}(f^2 - \omega_{eff}^2)}}\right)} \qquad \text{(A-2)}$$

with

$f = 2\Omega \sin\varphi$ Coriolis parameter

Ω rotational period of the earth

φ geographic latitude

$\omega_g = \frac{2\sqrt{\gamma - 1}}{\gamma}\omega_a$ Brunt-Väisälä frequency

The minus sign ($\nu = 1$) in Equation (A-2) is due to gravity waves, the plus sign ($\nu = 2$) is due to heat conduction waves.

In the treatment of turbulent waves we replace as a first order approximation the coefficient of molecular heat conductivity by a coefficient of eddy heat conductivity:

$$\kappa_{eddy} \sim L\kappa \qquad (L \sim 10^3)$$

In the range of our interest ($10^{-8} < \omega_{eff} < 10^{-7}$ sec^{-1}; $z < 100$ km) it is generally

$$\omega_h\, \omega_{eff} >> \begin{cases} \omega_a^2 \\ \dfrac{k_x^2 C^2 \omega_g^2}{f^2} \end{cases} \quad \text{and} \quad f >> \omega_{eff}.$$

Therefore approximate solutions of Equation (A-2) are

$$Ck_{z\nu} \sim \begin{cases} -j\sqrt{\omega_a^2 + \dfrac{k_x^2 C^2 \omega_g^2}{f^2}} & \text{(gravity waves)} \\ \sqrt{\omega_h\, \omega_{eff}}\,(1 - j) & \text{(heat conduction waves)} \end{cases} \qquad \text{(A-3)}$$

indicating that in this frequency range turbulent gravity waves are of an evanescent type. For $\omega_{eff} \rightarrow 0$ heat conduction waves too become evanescent waves ($C k_{z2} \rightarrow -j\omega_a$).

Appendix B

FULL WAVE THEORY AND RAY APPROXIMATION

Plane characteristic waves propagating through an inhomogeneous medium are coupled with each other. The real atmosphere is inhomogeneous for gravity waves and heat conduction waves because the vertical wave number k_z is a function of altitude via the term

$$\omega_h = \frac{\gamma c_p \bar{p}(z)}{\kappa_{eddy}} .$$

Therefore, full wave calculations are necessary to describe the wave propagation through the atmosphere.

The general solution of full wave analysis has the form (Volland, 1968b)

$$\mathbf{c}^i = \mathbf{P}^{ij} \mathbf{c}^j \qquad \text{(B-1)}$$

where

$$\mathbf{c}^i = \begin{pmatrix} \mathbf{a}^i \\ \mathbf{b}^i \end{pmatrix} = \begin{pmatrix} a_G^i \\ a_H^i \\ b_G^i \\ b_H^i \end{pmatrix}$$

is a column matrix containing the ascending ($\mathbf{a}^i$) and descending ($\mathbf{b}^i$) gravity waves (G) and heat conduction waves (H) in the altitude z_i and $\mathbf{P}^{ij}$ is a 4×4 matrix which connects the characteristic waves $\mathbf{c}$ in the altitudes z_i and z_j.

A rearrangement of the elements of P_i^j leads to reflection-, transmission-, conversion- and coupling coefficients:

$$R^i = \begin{pmatrix} {}_GR_G^i & {}_GR_H^i \\ {}_HR_G^i & {}_HR_H^i \end{pmatrix}; \quad T^i = \begin{pmatrix} {}_GT_G^i & {}_GT_H^i \\ {}_HT_G^i & {}_HT_H^i \end{pmatrix} \tag{B-2}$$

and equivalent expressions for R^j and T^j. Now the waves going into a layer are connected with the waves coming out of the layer by

$$\begin{pmatrix} b^i \\ a^j \end{pmatrix} = \begin{pmatrix} R^i & T^j \\ T^i & R^j \end{pmatrix} \begin{pmatrix} a^i \\ b^j \end{pmatrix}. \tag{B-3}$$

They are connected with the physical wave parameters like vertical velocity Δw, pressure Δp, temperature ΔT and temperature gradient $d\,\Delta T/dz$ by the relation

$$e = \frac{Q}{\sqrt{\bar{\rho}\,C}}\,c \tag{B-4}$$

where

$$e = \begin{pmatrix} \dfrac{\Delta w}{C} \\ \dfrac{\Delta p}{\bar{p}} \\ \dfrac{\Delta T}{\bar{T}} \\ \dfrac{\kappa\, d\,\Delta T/dz}{\bar{\rho}\,C} \end{pmatrix}$$

and

$$Q_{1\nu} = \left(q_\nu - jA + \frac{2jA\Lambda}{\gamma}\right) F_\nu$$

$$Q_{2\nu} = -(2A^2 + 2jAq_\nu) F_\nu$$

$$Q_{3\nu} = -(A^2 + q_\nu^2) F_\nu$$

$$Q_{4\nu} = \frac{\gamma}{(\gamma - 1) \cdot 2jG} (q_\nu + jA) \cdot Q_{3\nu}$$

$$q_\nu = k_{z\nu}/k \; ; \; q_3 = -q_1 \; ; \; q_4 = -q_2$$

$$k = \frac{\omega_{eff}}{C}$$

$$A = \frac{\omega_a}{\omega_{eff}}$$

$$\Lambda = \frac{k_x^2 \, C^2}{\omega_{eff}^2 - f^2}$$

$$G = \frac{\omega_h}{\omega_{eff}}$$

$$H = \frac{C^2}{\gamma \, g}$$

$$D_\nu = q_\nu^2 + A^2 + jG$$

$$F_\nu = \frac{1}{\sqrt{2q_\nu}} \exp\left\{ - \int_{z_1}^{z_j} \frac{(q_\nu^2 + A^2)}{4H} \left(\frac{jG}{D_\nu^2} - \frac{jA}{q_\nu D_\nu} \right) d\xi \right\}. \qquad \text{(B-5)}$$

Ray approximation is valid if the coupling between the different wave modes is weak enough so that reflection and conversion as well as coupling can be neglected ($R \sim 0$; ${}_HT_G = {}_GT_H \sim 0$). Then the transmission coefficients are approximately

$$\left.\begin{aligned} {}_GT_G^i &= - {}_GT_G^j \\ {}_HT_H^i &= - {}_HT_H^j \end{aligned}\right\} \sim \exp\left\{ - j \int_{z_1}^{z_j} k_{z\nu} \, d\xi \right\} \qquad (z_i \leqq z_j) \qquad \text{(B-6)}$$

With the special normalization of **Q** [(Equation (B-5)], Equation (B-6) in connection with Equation (B-4), is in fact the WKB-solution.

9. REFERENCES

Belrose, J. S., 1967: The "Berlin" warming, Nature 214, pp. 660-664

Bossolasco, M. and A. Elena, 1963: Absorption de la couche D et temperature de la mesosphere, Comt. Rend. 256, pp. 4491-4493

Cole, A. E. and A. J. Kantor, 1963: Air Force interim supplemental atmospheres to 90 km, Air Force Surveys in Geophysics No. 153

Finger, F. G. and S. Teweles, 1964: The mid-winter 1963 stratospheric warming and circulation change, J. Appl. Meteor. 3, pp. 1-15

Finger, F. G. and R. M. McInturff, 1968: Provision of Meteorological information for planning of SST flights, Paper presented at Commission for Aeronautical Meteorology, Technical Conference, London, England, March 1968 (to be published in Proceedings of Conference by WMO)

Fortak, H., 1958: Das Eindringen hochatmosphärischer Erwärmungen in die untere Stratosphäre als Austauschproblem, Gerland's Beiträge zur Geophysik, 67. pp. 66-78

Hirota, I. 1967a Dynamic Instability of the polar vortex, Journ. Meteor. Soc. Japan, 45, pp. 419-421

Hirota, I. 1967b The vertical structure of the stratospheric sudden warming, Journ. Meteor. Soc. Japan, 45, pp. 422-435

Johnson, K. W., 1968: Stratospheric Warming of 1967-1968, Journ. Geophys. Res., 73, p. 4775

Julian, P. R. and K. B. Labitzke, 1965: A study of atmospheric energetics during the January-February 1963 stratospheric warming, J. Atmos. Sci. 22, pp. 597-610

Kellogg, W. W., 1964: Pollution of the Upper Atmosphere by Rockets, Space Sci. Rev. 3, pp. 275-316

Labitzke, K. and H. Schwentek 1968: Midwinter Warmings in the Stratosphere and Lower Mesosphere and the Behaviour of Ionospheric Absorption, Paper presented at the XIth COSPAR Meeting, Tokyo, 1968; Beilage zur Berliner Wetterkarte 115/68, Institute für Meteorologie and Geophysik der Freien Universität Berlin, Germany; to be published also: Space Research IX, North Holland Publishing Company, Amsterdam

Lauter, E. A., 1967: Present research aspects in ionospheric -stratospheric coupling effects, Space Research VII, North-Holland Publishing Company, Amsterdam, pp. 212-227

Matsuno, T. and I. Hirota, 1966: On the dynamic stability of polar vortex in wintertime, Journ. Meteor. Soc. Japan, Series II, 44, pp. 122-128

Miyakoda, K., R. F. Strickler, and G. D. Hembree 1968: Numerical Simulation

of the Breakdown of the Polar-night Vortex in the Stratosphere, I. Manuscript, to be published.

Newell, R. G., 1963: Preliminary Study of Quasi Horizontal Eddy Fluxes from Meteorological Rocket Network Data, Journ. Atm. Sci. 20, pp. 213-225

Perry, J. S., 1967: Long wave energy processes in the 1963 sudden stratospheric warming, J. Atmos. Sci. 24, pp. 539-550

Regener, E., 1952: Zur Erklärung der Warmlufteinbrüche in die untere Stratosphäre, Bericht d. DWD, 38, p. 289

Scherhag, R., 1952: Die explosionsartigen Stratosphärenerwärmungen des Spätwinters 1951/52, Bericht des DWD, 38, p. 51

Scherhag, R. et al., 1963-1966: Meteorologische Abhandlungen des Instituts für Meteorologie und Geophysik der Freien Universität Berlin, Verlag Reimer, Berlin, Band 37 - 40

Sechrist, C. F., 1967: A theory of the winter absorption anomaly at middle latitudes, Journ. Atm. Terr. Phys. 29, pp. 113-136

Sechrist, C. F., Mechtly, E. A., Shirke, J. S. and J. S. Theon 1968: Coordinated Rocket measurements on the D-region winter anomaly, I. Experimental results, to be published in Journ. Atm. Terr. Phys.

Shapley, A. H. and W. J. G. Beynon, 1965: Winteranomaly in the ionospheric absorption and stratospheric warmings, Nature 206, pp. 1242-1243

Smith, W. S., Theon, J. S., Swartz, P. C., Katchen, T. B. and J. J. Horvath, 1967: Temperature pressure, density and wind measurements in the upper stratosphere and mesosphere, 1965: NASA Technical Report, NASA TR R-263, September 1967

Volland, H., 1968a: The upper atmosphere as a multiple refractive medium for neutral air motions, to be published in Journ. Atm. Terr. Phys.

Volland, H., 1968b: Full wave calculations of thermospheric neutral air motions, NASA Document X 621-68-176 GSFC, Greenbelt, Md.

Warnecke, G., 1962: Über die Zustandsänderungen der nordhemisphärischen Stratosphäre, Meteorologische Abhandlungen, Vol. 28, 3, Institute für Meteorologie nd Geophysik der Freien Universität Berlin, Germany

Warnecke, G., 1968: Untersuchungen der Zirkulation der, oberen Stratosphäre und der unteren Mesosphäre, (manuscript, to be published in METEOROLOGISCHE ABHANDLUNGEN, Berlin)

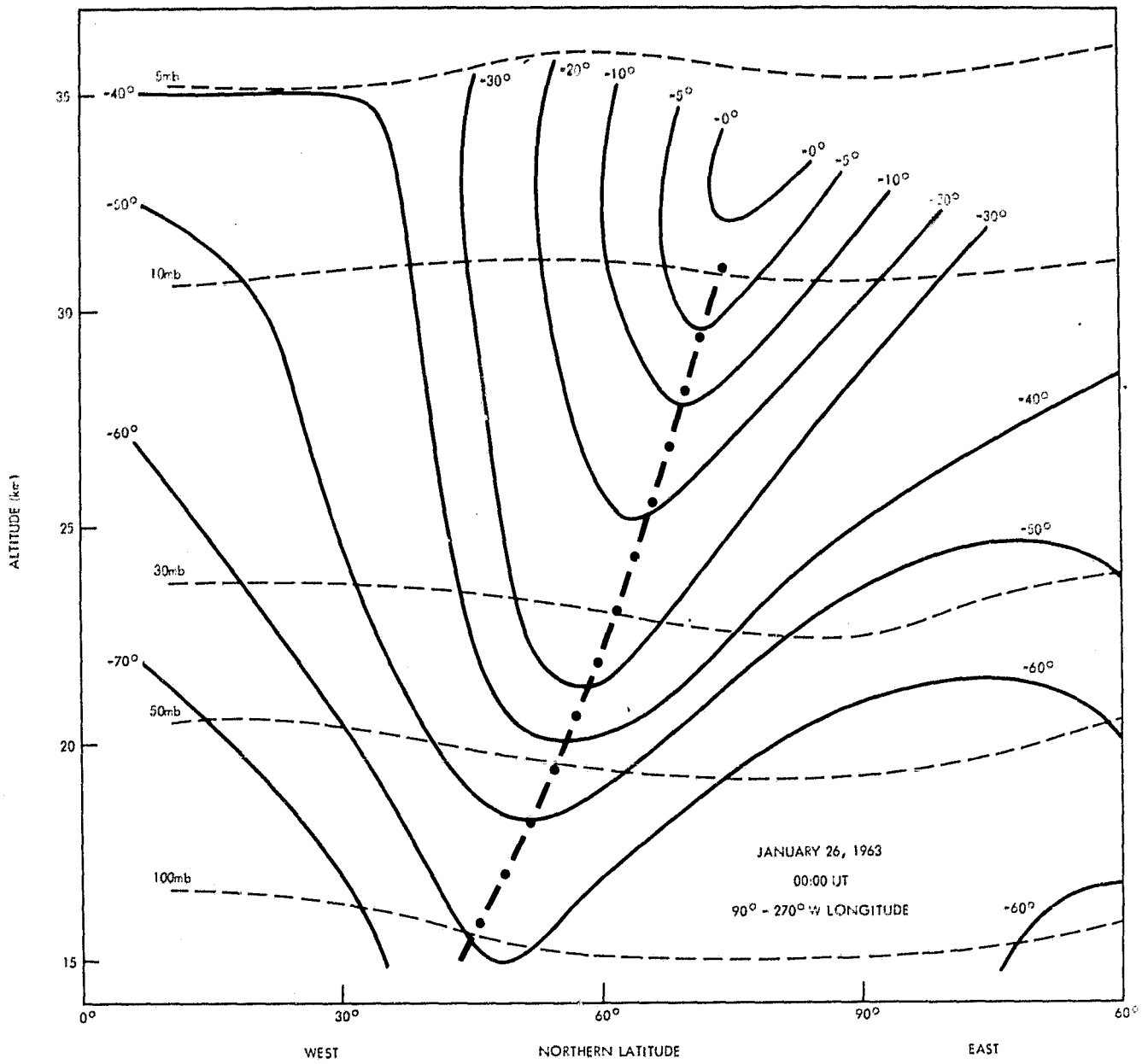

Figure 1a. Cross-section of Temperature (solid lines) and pressure (dashed lines) along 90°W and 90°E on 26 January 1963 derived from stratospheric weather maps (METEOROLOGISCHE ABHANDLUNGEN 1963-1966). The dashed-dotted line represents a calculated plane of equal phase of heat conduction waves.

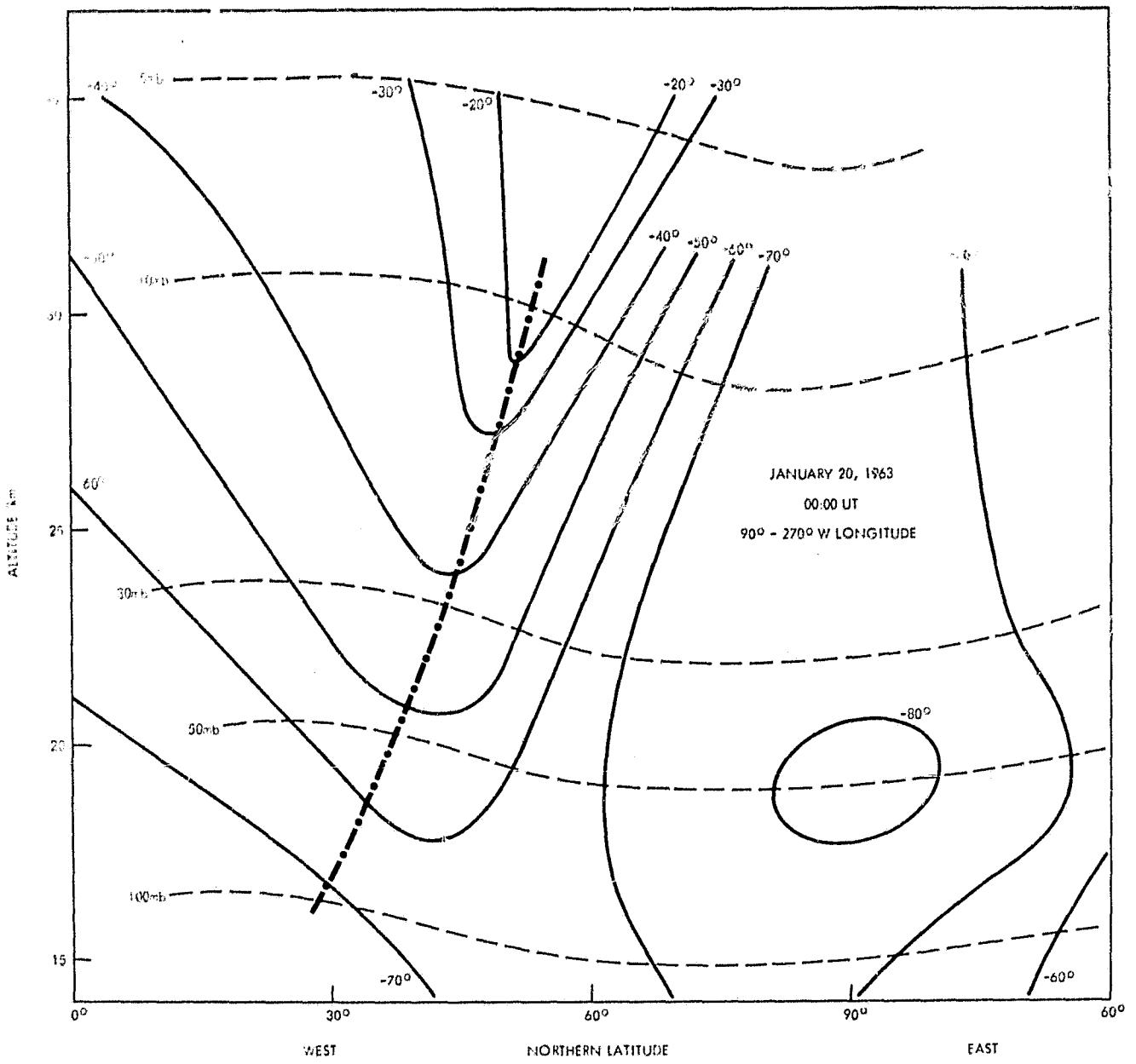

Figure 1b. Cross-section of Temperature (solid lines) and pressure (dashed lines) along 90°W and 90°E on 20 January 1963 derived from stratospheric weather maps (METEOROLOGISCHE ABHANDLUNGEN 1963-1966). The dashed-dotted line represents a calculated plane of equal phase of heat conduction waves.

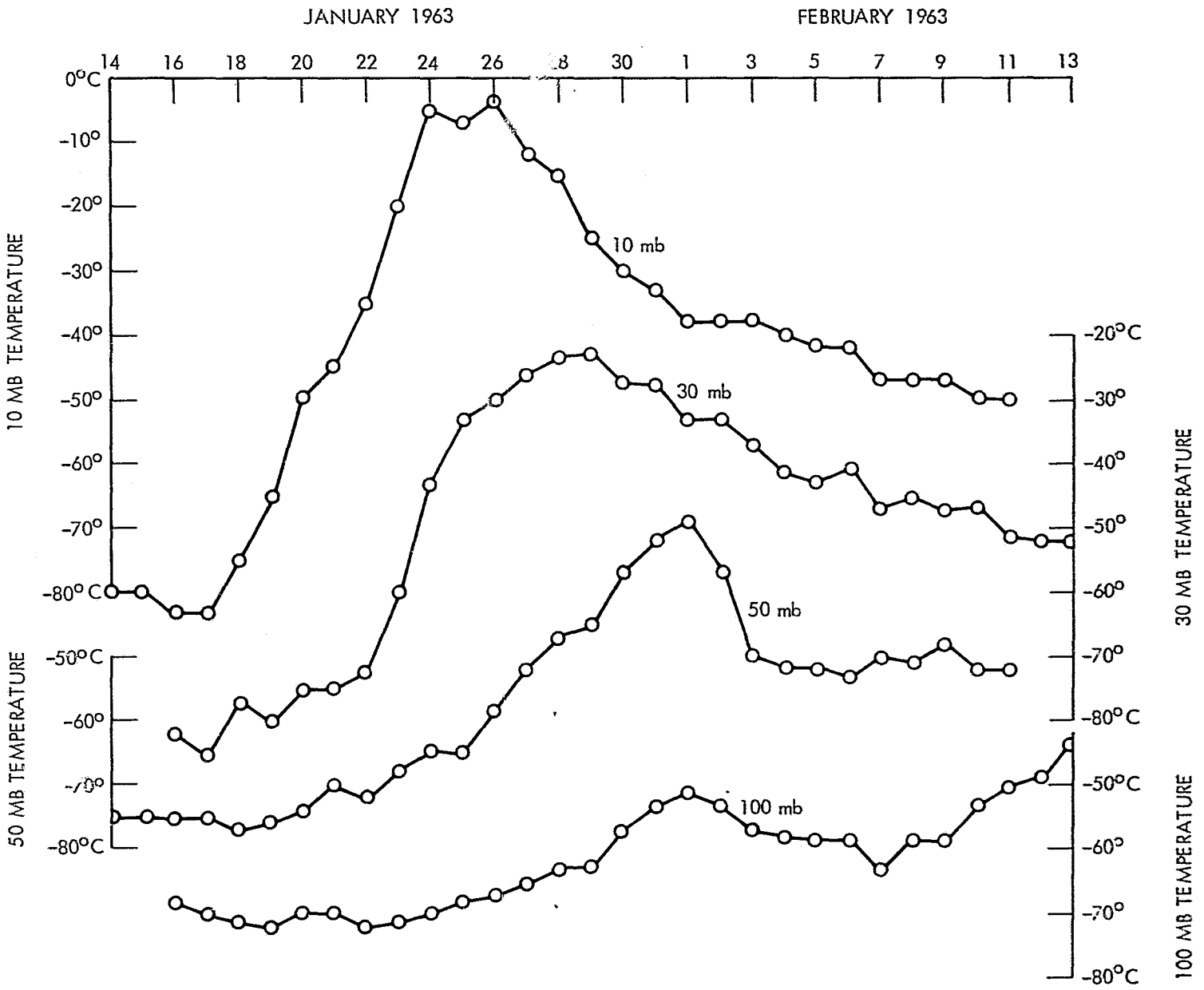

Figure 2. Temperature variation with time at different isobaric levels at 70°N and 90°W during the January 1963 stratospheric warming, derived from stratospheric weather maps (METEOROLOGISCHE ABHANDLUNGEN 1963-1966)

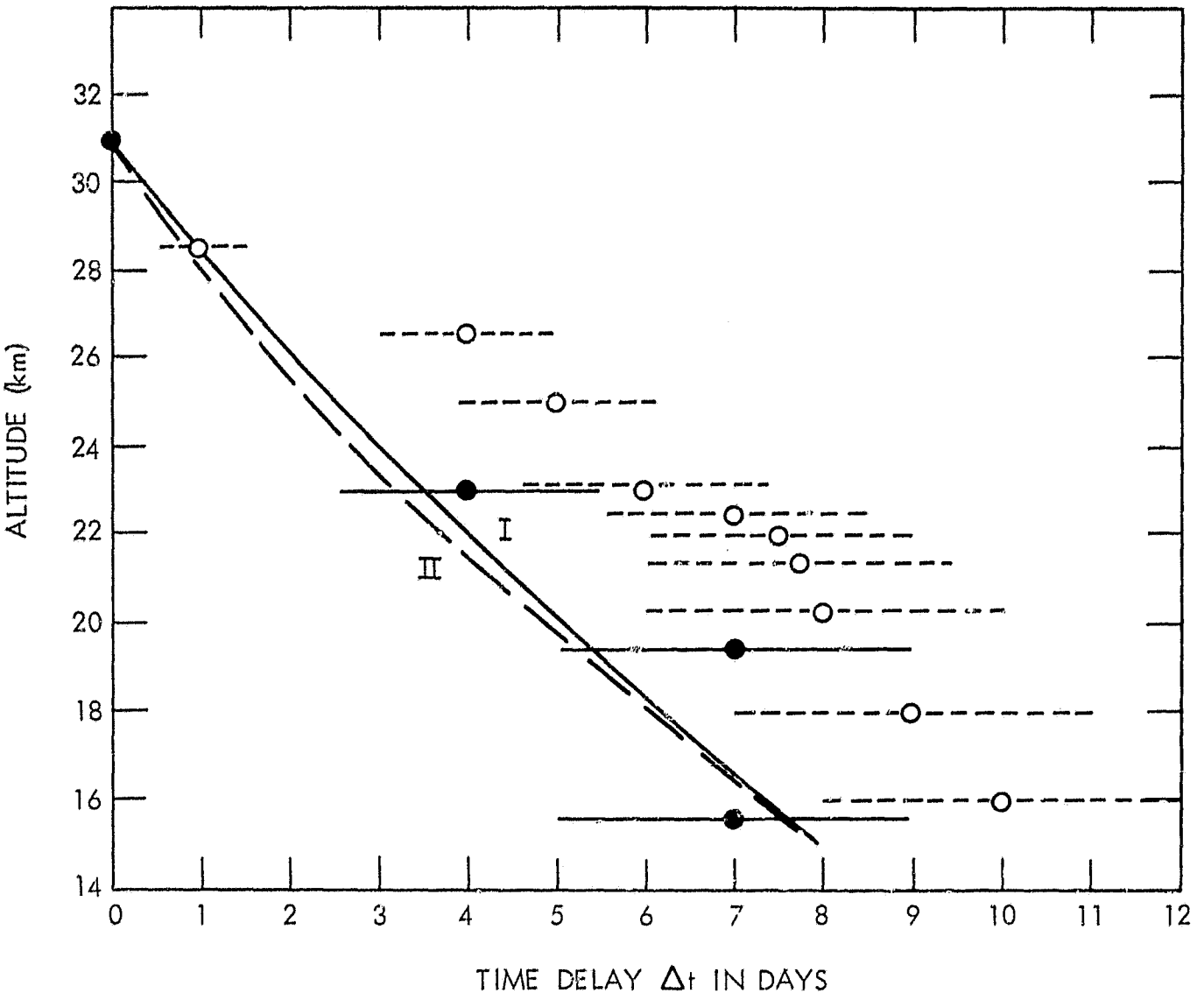

Figure 3. Time delay Δt versus height of the occurrence of the temperature maximum during the 1963 stratospheric warming (solid circles) derived from Figure 2. Open circles represent corresponding values derived for the February 1952 event. Horizontal bars indicate range of uncertainty of the derived data. Solid curve (I) and dashed curve (II) were computed with the following parameters:

ω	$7 \times 10^{-6}\ \text{sec}^{-1}$	$5 \times 10^{-6}\ \text{sec}^{-1}$
ω_{eff}	$4.6 \times 10^{-8}\ \text{sec}^{-1}$	$2.2 \times 10^{-8}\ \text{sec}^{-1}$
k_x	$1.5 \times 10^{-3}\ \text{km}^{-1}$	$1.0 \times 10^{-3}\ \text{km}^{-1}$

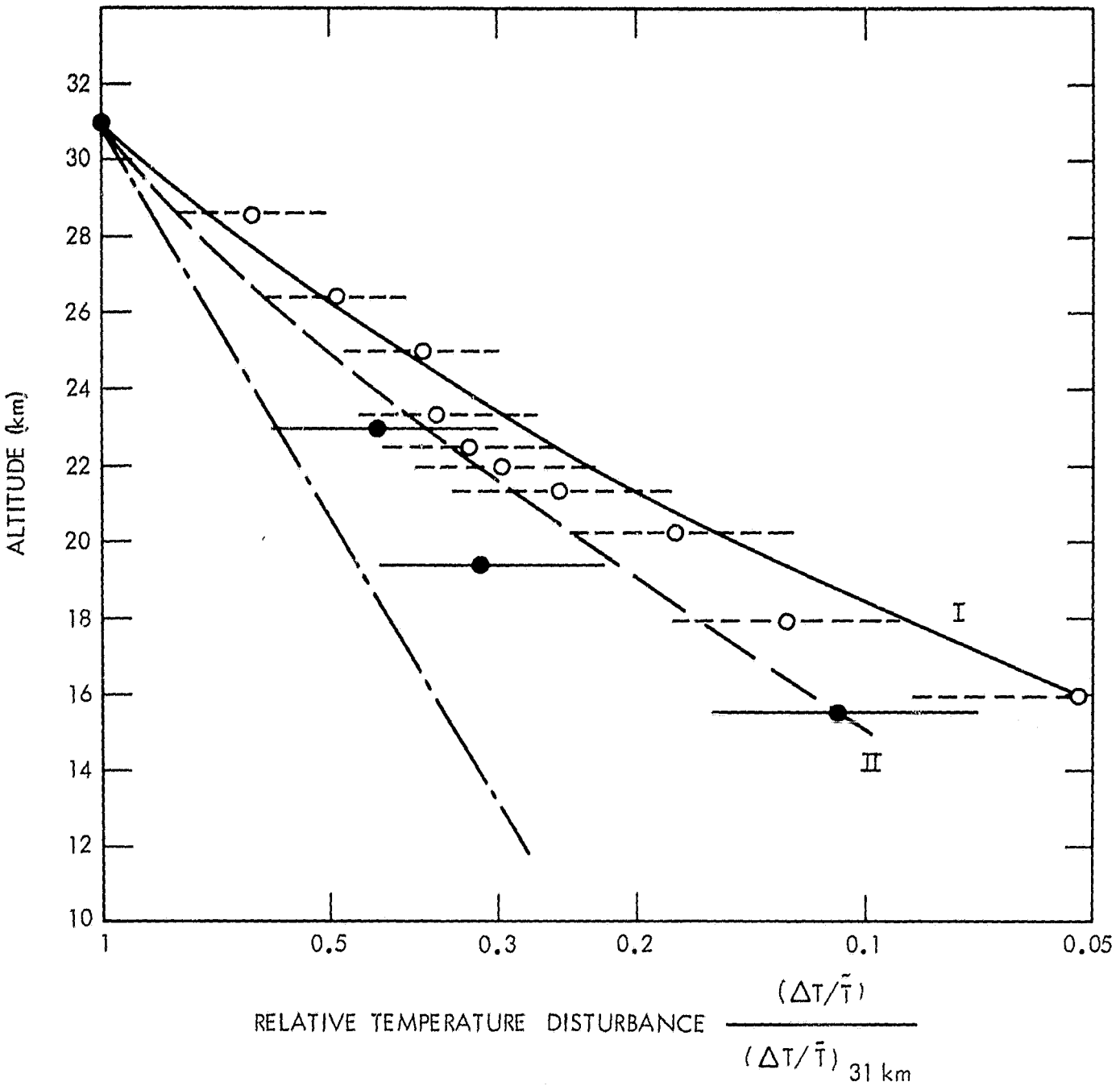

Figure 4. Relative amplitude of temperature disturbance as function of height. The January 1963 data (solid circles) were derived from Figure 2. Open circles represent corresponding data for the February 1952 event. Horizontal bars indicate range of uncertainty. The solid (I) and dashed (II) curves have been calculated with the same parameters listed in Figure 3. The dashed-dotted line represents the lower limit of amplitude decrease for a nondissipative wave.

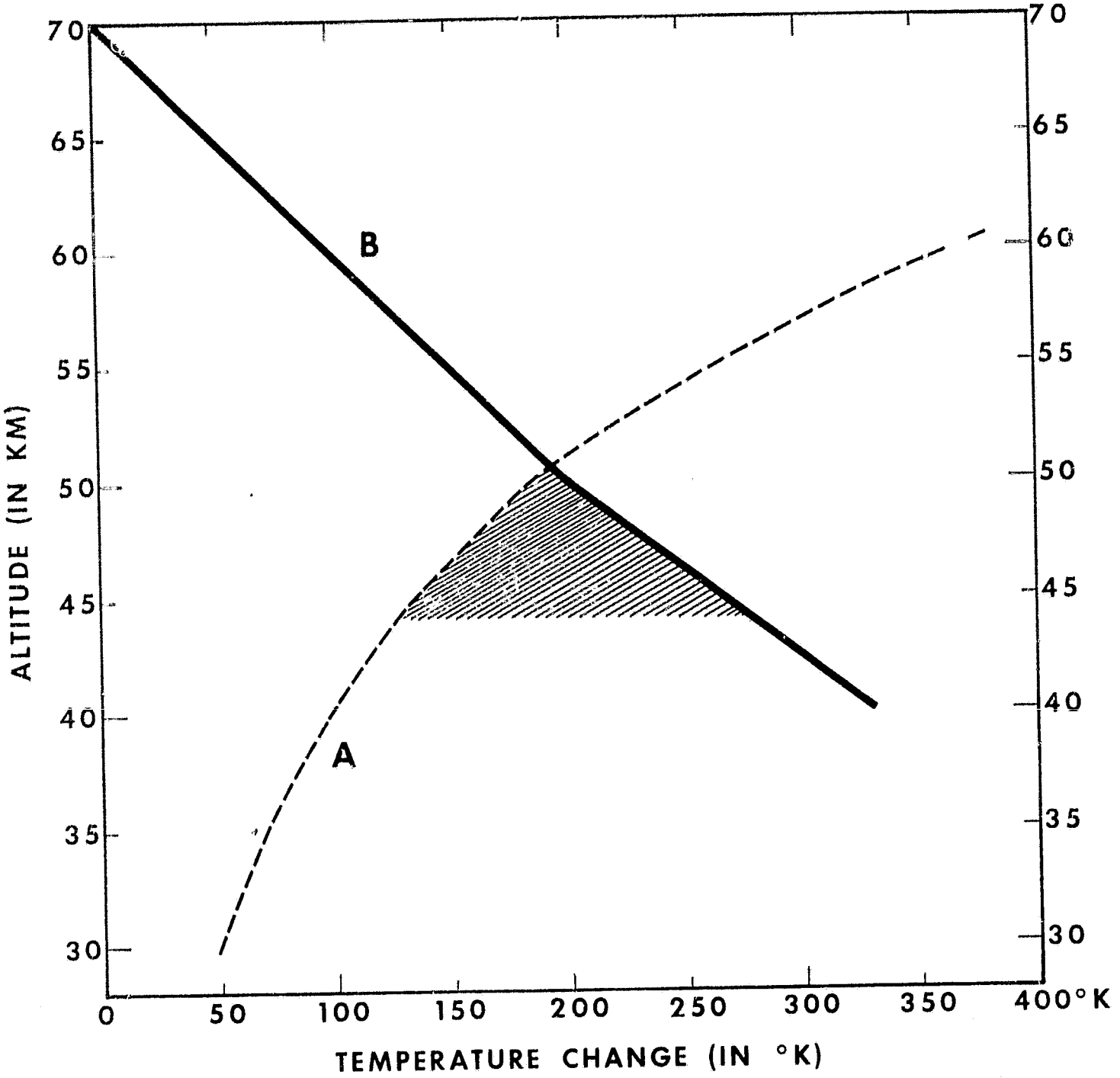

Figure 5. Minimum change of temperature amplitude (Curve A), as a function of altitude, required to explain a temperature increase of 50°K at 30 km after Equation (12); and maximum permissive temperature increase (Curve B) as function of altitude in an isothermal mesosphere, between 70 km and 50 km, and a colder upper stratosphere (below 50 km). The hatched area delineates the area of most probable origin of the initial heat impulse.

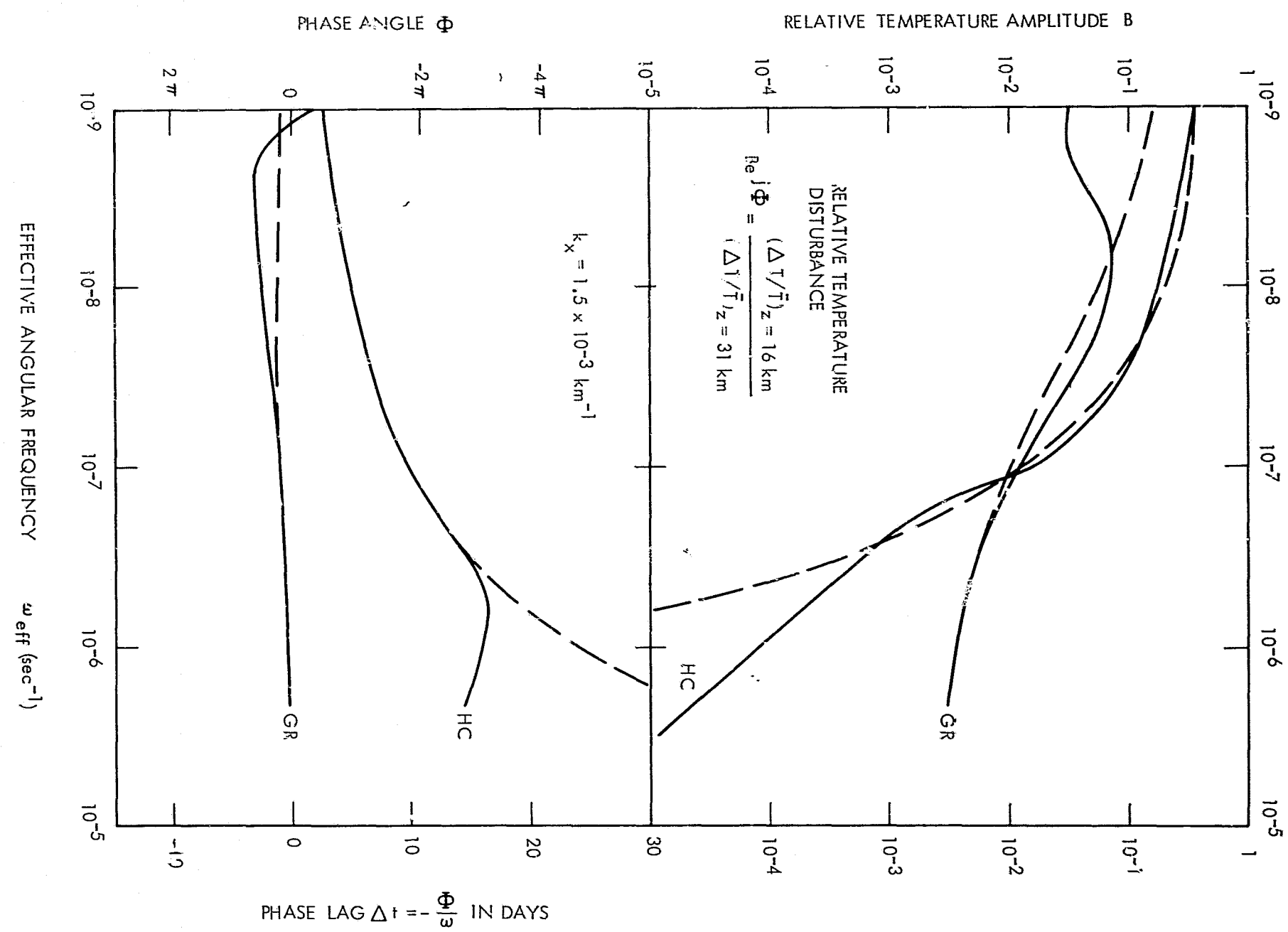

Figure 6. Amplitude (a) and phase (b) of relative temperature disturbance at 16 km altitude as a function of angular frequency ω_{eff} (in sec^{-1}) for initial gravity waves (GR) and initial heat conduction waves (HC) at 31 km. Solid curves resulted from full wave calculation, dashed curves from ray approximation. The horizontal wave number is $k_x = 1.5 \times 10^{-3}\,km^{-1}$.

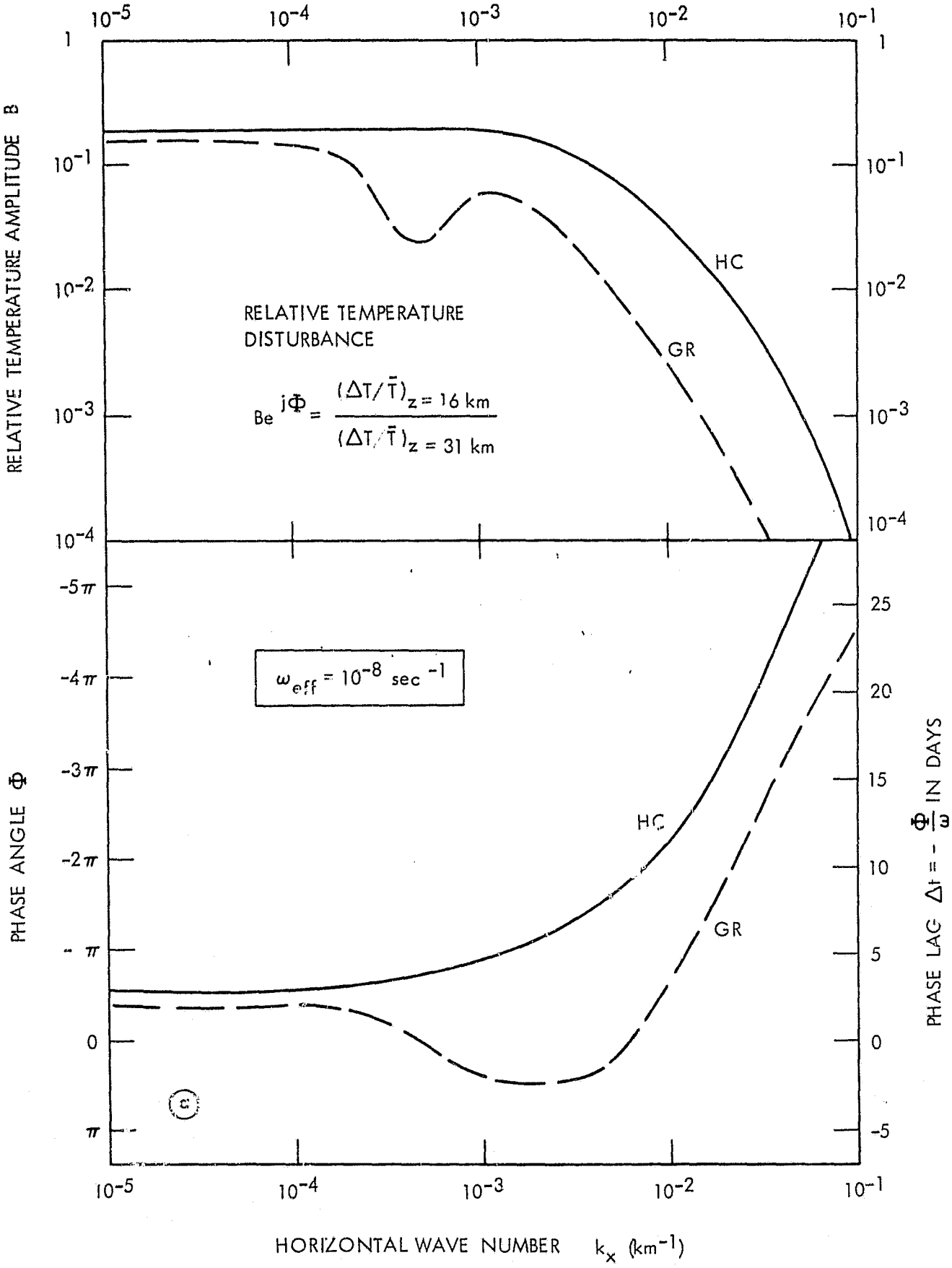

Figure 7. Amplitude and phase of relative temperature disturbance at 16 km altitude as a function of horizontal wave number k_x (in km^{-1}) for initial gravity waves (GR) and initial heat conduction waves (HC) at 31 km altitude for two different effective angular frequencies ω_{eff} (in sec^{-1}).

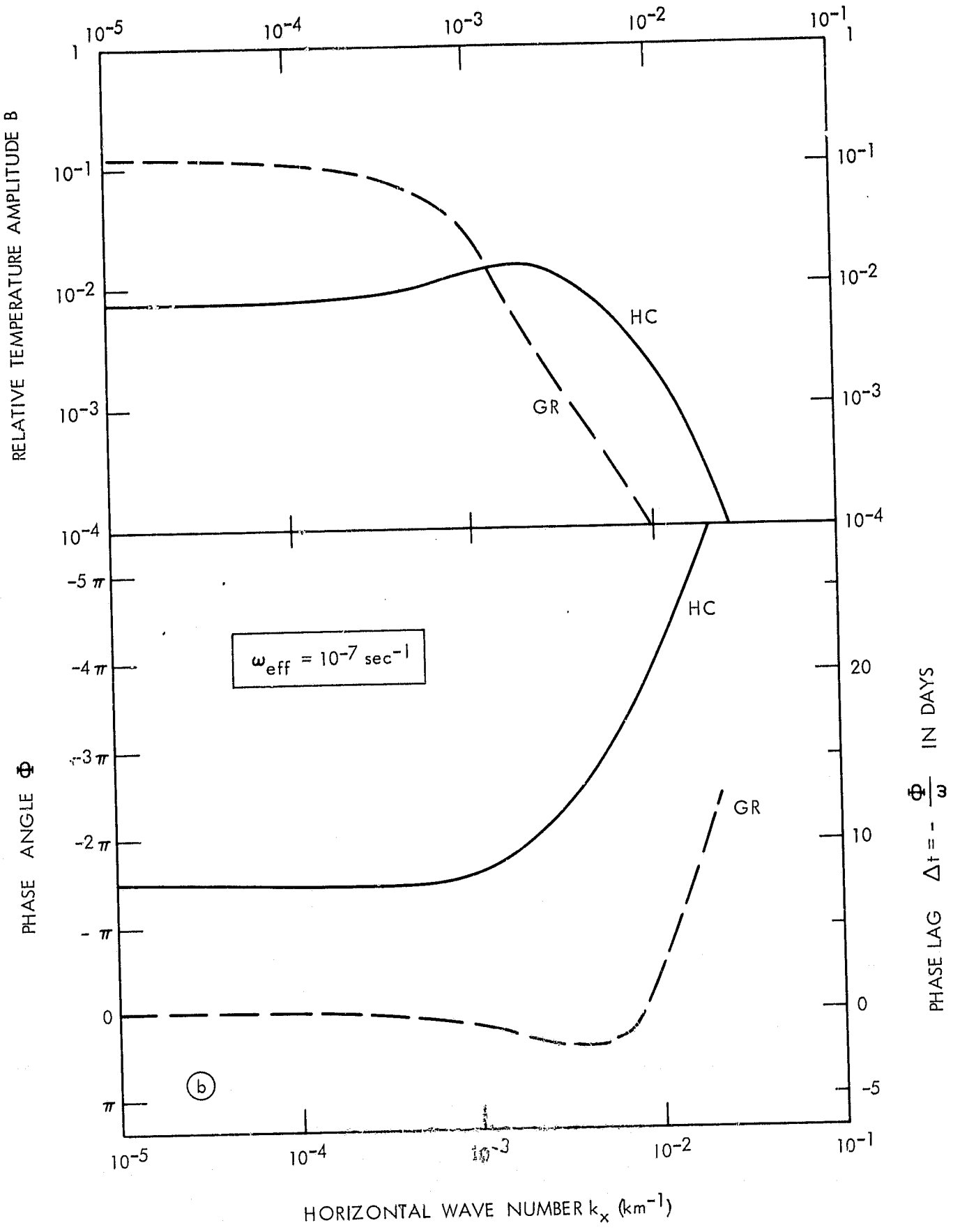
RELATIVE TEMPERATURE AMPLITUDE B
PHASE ANGLE Φ
PHASE LAG Δt = - Φ/ω IN DAYS
HORIZONTAL WAVE NUMBER k_x (km^{-1})
10^{-5}
10^{-4}
10^{-3}
10^{-2}
10^{-1}
1
-5π
-4π
-3π
-2π
$-\pi$
0
π
20
10
-5
HC
GR
$\omega_{eff} = 10^{-7}$ sec^{-1}
(b)

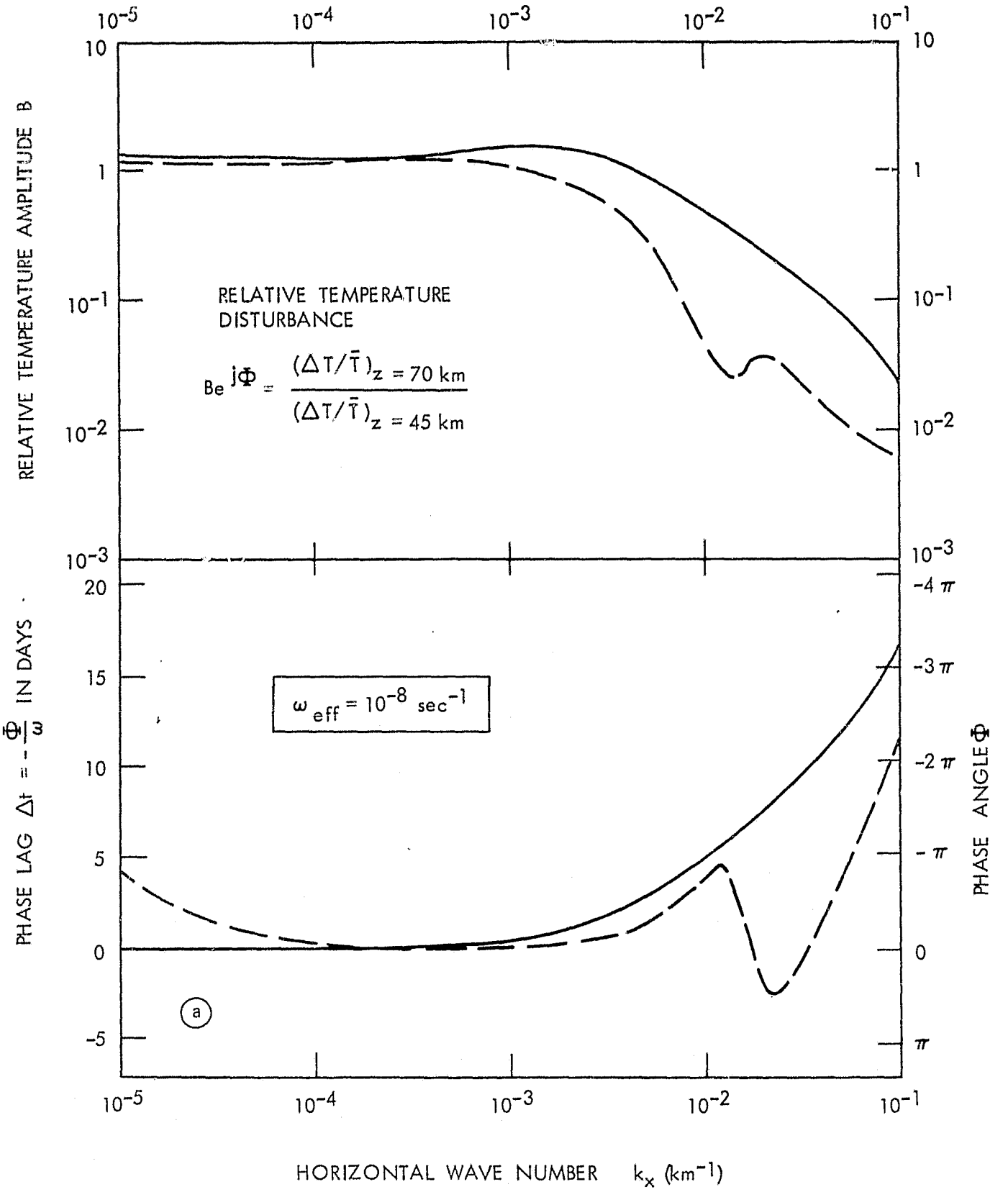

Figure 8. Amplitude and phase of relative temperature disturbance at 70 km altitude as a function of horizontal wave number k_x (in km^{-1}) for initial gravity waves (GR) and initial heat conduction waves (HC) at 45 km altitude for two different effective angular frequencies ω_{eff} (in sec^{-1}).

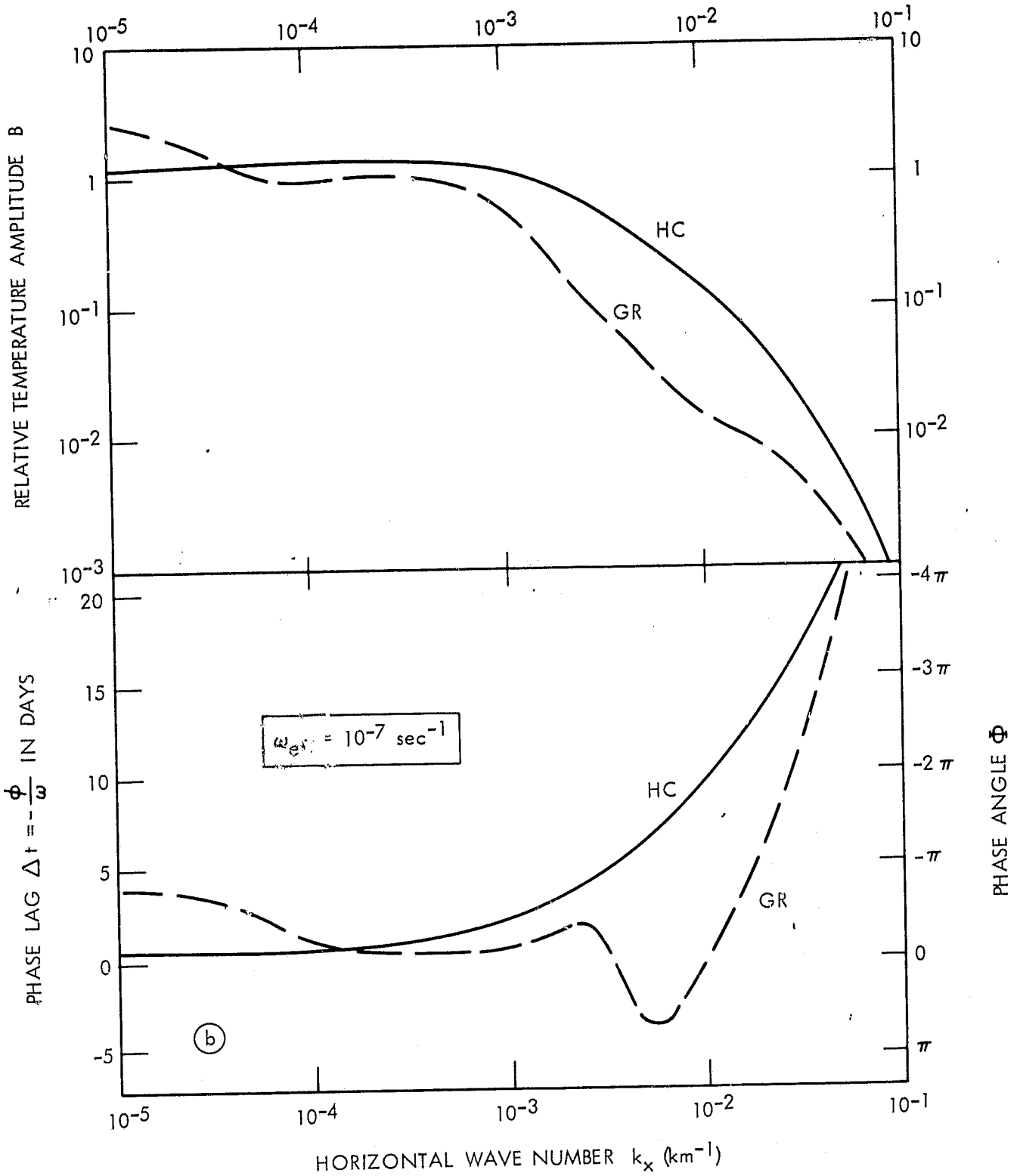
RELATIVE TEMPERATURE AMPLITUDE B
PHASE LAG $\Delta t = -\frac{\phi}{\omega}$ IN DAYS
PHASE ANGLE Φ
HC
GR
$\omega_{est} = 10^{-7}$ sec^{-1}
b
HORIZONTAL WAVE NUMBER k_x (km^{-1})
10^{-5}
10^{-4}
10^{-3}
10^{-2}
10^{-1}
10
1
10^{-1}
10^{-2}
10^{-3}
20
15
10
5
0
-5
-4π
-3π
-2π
$-\pi$
0
π

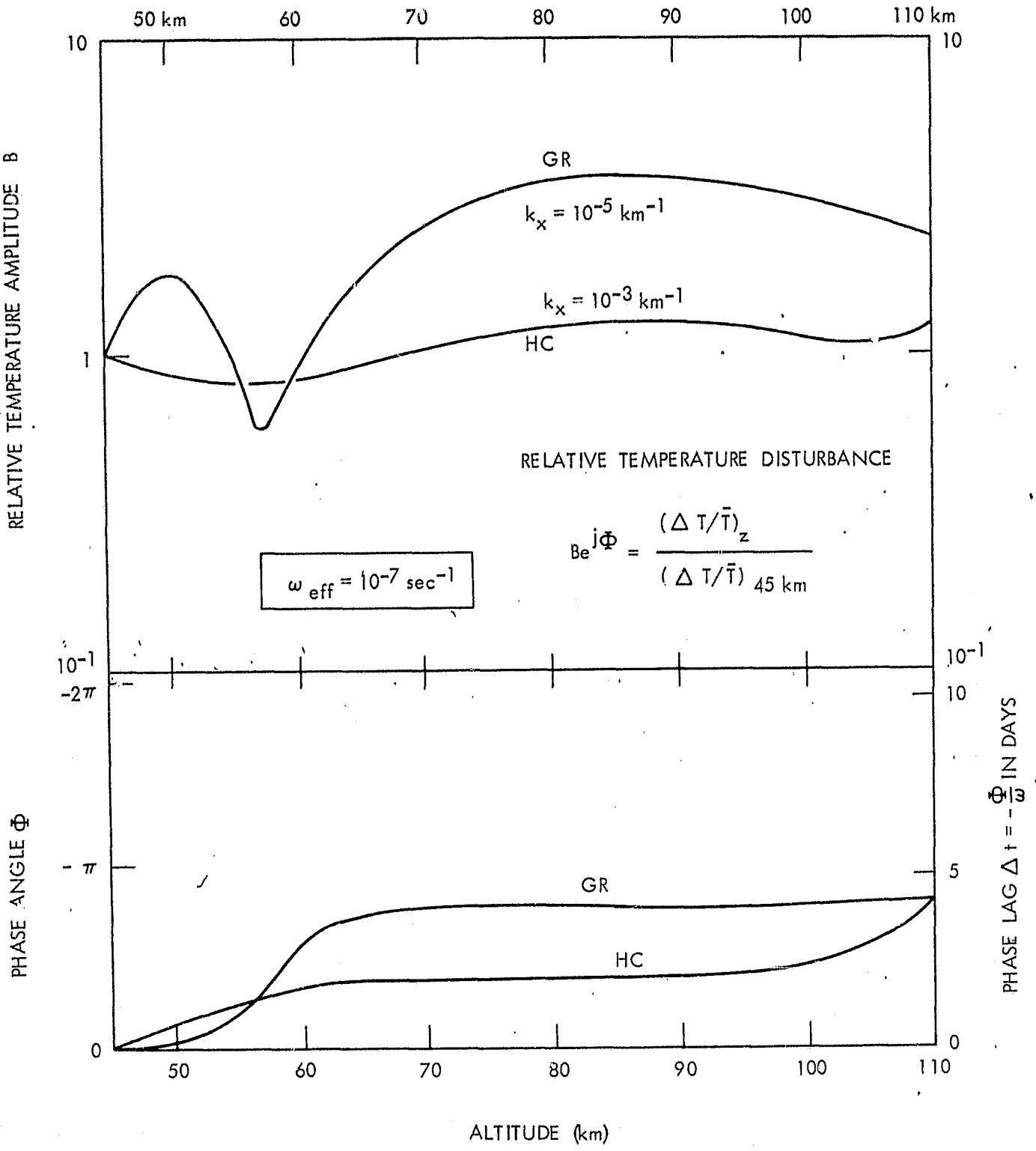

Figure 9. Amplitude and phase of relative temperature disturbance as a function of height for initial gravity waves (GR) and initial heat conduction waves (HC) at 45 km altitude. The effective angular frequency is $\omega_{eff} = 10^{-7}$ sec^{-1}.